


Entanglement enhanced metrology with quantum many-body scarsShane Dooley^{1,*}, Silvia Pappalardi^{2,†} and John Goold^{1,‡}¹*Department of Physics, Trinity College Dublin, Dublin 2, Ireland*²*Laboratoire de Physique de l'École Normale Supérieure, ENS, Université PSL, CNRS, Sorbonne Université, Université de Paris, F-75005 Paris, France* (Received 15 August 2022; revised 7 December 2022; accepted 8 January 2023; published 17 January 2023)

Although entanglement is a key resource for quantum-enhanced metrology, not all entanglement is useful. For example, in the process of many-body thermalization, bipartite entanglement grows rapidly, naturally saturating to a volume law. This type of entanglement generation is ubiquitous in nature but has no known application in most quantum technologies. The generation, stabilization, and exploitation of genuine multipartite entanglement, on the other hand, is far more elusive yet highly desirable for metrological applications. Recently, it has been shown that quantum many-body scars can have extensive multipartite entanglement. However, the accessibility of this structure for real application has been so far unclear. In this work, we show how systems containing quantum many-body scars can be used to dynamically generate stable multipartite entanglement and describe how to exploit this structure for phase estimation with a precision that beats the standard quantum limit. Key to this is a physically motivated modification of a Hamiltonian that generates a variety of multipartite entangled states through the dynamics in the scar subspace.

DOI: [10.1103/PhysRevB.107.035123](https://doi.org/10.1103/PhysRevB.107.035123)**I. INTRODUCTION**

When a simple initial condition is evolved with a generic locally interacting many-body Hamiltonian, local observables are expected to thermalize [1,2]. As a consequence of the evolution, entanglement entropy grows rapidly, saturating at a volume law [3–5] consistent with the thermal stationary value. This type of entanglement scaling, despite being ubiquitous [6], is known not to be useful in many quantum technologies [7]. On the other hand, multipartite entanglement—witnessed by the quantum Fisher information (QFI) [8–10]—is well known to be a crucial resource for quantum-enhanced metrology [11–15]. In fact, the use of highly multipartite entangled states allows one to overcome classical limitations in quantum phase-estimation protocols [12,16]. However, generally speaking, the fundamental challenge in creating and maintaining such states is that the dynamics of locally interacting many-body systems are thermalizing, which leads to states that are “too entangled to be useful” [7].

The usual approach to solving the problem of thermalization is to isolate every particle as much as possible, suppressing all unwanted interactions with other particles and with the wider environment. This approach has drawbacks: It can be difficult for large systems and often requires the particles to be spatially well separated, limiting the overall size of the multipartite entangled state. Recent experimental [17–20] and theoretical [21–23] work has uncovered a new mechanism—weak ergodicity breaking—that can prevent thermalization in nonintegrable many-body systems. At the heart of this mechanism are quantum many-body scars

(QMBS)—rare, nonthermal eigenstates in a spectrum of otherwise thermal eigenstates. The theoretical properties of these eigenstates are currently an active area of research [21–29]. For instance, although they display subvolume bipartite entanglement, it was recently shown that QMBS can have a nontrivial multipartite entanglement structure, embodied by an extensive scaling of the quantum Fisher information density [30]. This raises the tantalizing possibility of exploiting QMBS to dynamically generate multipartite entangled states, even in strongly interacting many-body systems. It is not practical to prepare a high-energy eigenstate of a strongly interacting many-body system in the laboratory so at first glance it would seem difficult to try to exploit this entanglement structure for quantum-enhanced metrology. However, one can aim to generate multipartite entangled states in the subspace spanned by the QMBS. Indeed, QMBS have been discussed in connection to spin squeezing in Refs. [32,33], but no protocol has been devised which directly exploits the robustness of multipartite entanglement in the QMBS subspace.

The main result of this work is to offer a prescription for robust multipartite entanglement generation through time evolution, even in the presence of local interactions that would usually be expected to lead to thermalization. Furthermore, we demonstrate how this structure can be exploited for quantum-enhanced metrology, building on previous work showing robust quantum sensing with separable states [31]. The key is QMBS, which enable us to overcome the notorious fragility of multipartite entanglement to local interactions. Another key component is a Hamiltonian modification that dynamically generates multipartite entanglement in the scar subspace. Illustrating the idea with an example, we show that much larger multipartite entangled states can be generated in models with QMBS, in comparison to similar models without QMBS. To show the potential for quantum technologies, we propose a metrological scheme for phase estimation. Again,

*shdooley@tcd.ie

†silvia.pappalardi@ens.phys.fr

‡gooldj@tcd.ie

we see significantly better estimation precision in a model with QMBS, compared to a similar model without QMBS.

II. EXACT MANY-BODY SCARS AND MULTIPARTITE ENTANGLEMENT

Mark *et al.* [34] proposed a general framework for models with QMBS, called the spectrum-generating algebra (SGA) framework [35,36]. The main ingredients are a linear subspace $\mathcal{S} \subset \mathcal{H}$ of the Hilbert space and an operator \hat{Q}^+ that obeys the following properties: (i) \hat{Q}^+ preserves the subspace \mathcal{S} , i.e., $(\hat{\mathbb{I}} - \hat{\mathcal{P}}_S)\hat{Q}^+\hat{\mathcal{P}}_S = \hat{\mathcal{P}}_S\hat{Q}^+(\hat{\mathbb{I}} - \hat{\mathcal{P}}_S) = 0$, where $\hat{\mathcal{P}}_S$ is the projector into \mathcal{S} , and (ii) \hat{Q}^+ is a raising operator in \mathcal{S} , i.e.,

$$\hat{\mathcal{P}}_S([\hat{H}, \hat{Q}^+] - \omega\hat{Q}^+)\hat{\mathcal{P}}_S = 0. \quad (1)$$

If the subspace \mathcal{S} contains a Hamiltonian eigenstate $|\mathcal{S}_0\rangle \in \mathcal{S}$, with $\hat{H}|\mathcal{S}_0\rangle = E_0|\mathcal{S}_0\rangle$, then the states $|\mathcal{S}_j\rangle = \mathcal{N}_j(\hat{Q}^+)^j|\mathcal{S}_0\rangle \in \mathcal{S}$ (where \mathcal{N}_j is a normalization factor) are also Hamiltonian eigenstates, $\hat{H}|\mathcal{S}_j\rangle = (E_0 + j\omega)|\mathcal{S}_j\rangle$. When the Hamiltonian \hat{H} is found to be nonintegrable (e.g., through analysis of the energy level spacing statistics [21]), these states $|\mathcal{S}_j\rangle$ are regarded as quantum many-body scars. We note that the SGA condition in Eq. (1) is closely related to the condition for a dynamical symmetry that was introduced in Refs. [37,38].

It was recently shown that the scars have extensive multipartite entanglement, in contrast to the thermal eigenstates that make up the remainder of the spectrum of \hat{H} . The degree of multipartite entanglement of a quantum state $\hat{\rho}$ can be probed with the quantum Fisher information (QFI) [39–41]:

$$\mathcal{F}(\hat{O}, \hat{\rho}) = 2 \sum_{n,m} \frac{(p_n - p_m)^2}{p_n + p_m} |n|\hat{O}|m\rangle|^2 \leq 4\text{Var}_{\hat{\rho}}\hat{O}, \quad (2)$$

with respect to an appropriately chosen observable \hat{O} . Here, p_n , $|n\rangle$ are the eigenvalues and eigenstates of $\hat{\rho}$ and the upper bound $\text{Var}_{\hat{\rho}}\hat{O} = \text{Tr}(\hat{O}^2\hat{\rho}) - [\text{Tr}(\hat{O}\hat{\rho})]^2$ is achieved for pure states $\hat{\rho} = |\psi\rangle\langle\psi|$. For an N -particle system and a collective observable $\hat{O} = \frac{1}{2} \sum_{n=1}^N \hat{o}_n$ (sum of local ones \hat{o}_n), a QFI density satisfying

$$f(\hat{O}, \hat{\rho}) \equiv \frac{\mathcal{F}(\hat{O}, \hat{\rho})}{N} > m \quad (3)$$

indicates that at least $m + 1$ particles of the system are entangled [8–10]. Importantly, the QFI is also a key quantifier of the usefulness of the state $\hat{\rho}$ in quantum metrology [11,14,15]: The precision in estimating a parameter ε , encoded in the state $\hat{\rho}_\varepsilon = e^{-i\varepsilon\hat{O}}\hat{\rho}e^{i\varepsilon\hat{O}}$, is bounded by the Cramér-Rao inequality $\delta\varepsilon \geq 1/\sqrt{\nu\mathcal{F}}$, where ν is the number of independent repetitions of the measurement. Hence, while phase sensitivity with a separable state is bounded by the *standard quantum limit* $\delta\varepsilon \geq \delta\varepsilon_{\text{SQL}} = 1/\sqrt{\nu N}$, the presence of multipartite entanglement results in an enhancement up to $\delta\varepsilon \geq \delta\varepsilon_{\text{HL}} = 1/\sqrt{\nu N}$, known as the *Heisenberg limit* [12,16]. Recently, the QFI has been studied theoretically and experimentally in many-body systems due to its relation to thermal susceptibilities [42–47]. However, in the case of locally interacting Hamiltonians, it is generally very challenging to generate quantum states with the Heisenberg scaling.

Reference [30] showed that any QMBS with nonzero energy density has a QFI density with exactly this property: Extensive $f \sim N$, while for thermal eigenstates $f \sim 1$. Despite the extensive multipartite entanglement of the QMBS, dynamics through the scar subspace are often through states with low entanglement. This is because, typically, the system is initialized in an easily prepared separable (or low-entanglement) state, and dynamics through the scar subspace does not significantly change the entanglement structure. In order to see this, we note that Eq. (1) above implies that the Heisenberg equation of motion for the operator $\hat{Q}_S^+ \equiv \hat{\mathcal{P}}_S\hat{Q}^+\hat{\mathcal{P}}_S$ is linear inside the scarred subspace, $\frac{d}{dt}\hat{Q}_S^+(t) = i\omega\hat{Q}_S^+(t) \Rightarrow \hat{Q}_S^+(t) = \hat{Q}_S^+(0)e^{i\omega t}$. Assume that the initial state is a generalized coherent state $|\theta, \phi\rangle \equiv \hat{D}(\theta, \phi)|\mathcal{S}_0\rangle$, where $\hat{D}(\theta, \phi) = \exp\{\frac{\theta}{2}(\hat{Q}^+e^{-i\phi} - \hat{Q}^-e^{i\phi})\}$ is the unitary “displacement” operator and $\hat{Q}^- = (\hat{Q}^+)^\dagger$. Such a state is a superposition of QMBS, without any overlap with the other thermal eigenstates. Then, due to the linearity of the equation of motion for \hat{Q}_S^+ , the time-evolved state is

$$|\psi(t)\rangle = e^{-it\hat{H}}|\theta, \phi\rangle = e^{-itE_0}|\theta, \phi - \omega t\rangle, \quad (4)$$

i.e., the time-evolved state is always a generalized coherent state in the QMBS subspace. If the coherent state displacement operator $\hat{D}(\theta, \phi)$ can be expressed as a product of local unitaries (as is often the case), then every coherent state $|\theta, \phi\rangle = \hat{D}(\theta, \phi)|\mathcal{S}_0\rangle$ has the same entanglement structure as $|\mathcal{S}_0\rangle$. In particular, if $|\mathcal{S}_0\rangle$ has low entanglement, then the time-evolving state $|\psi(t)\rangle$ will too. We also note that the evolving state undergoes periodic revivals to the initial state with a period $T = 2\pi/\omega$, which is characteristic of most examples of dynamics in scarred many-body systems up to now.

In order to generate multipartite entangled states in the scarred subspace \mathcal{S} , we consider adding a term

$$\hat{H}_{\text{nl}} = \frac{\chi}{N}\hat{Q}^+\hat{Q}^- \quad (5)$$

to a Hamiltonian that possesses a scarred subspace. Here, N is the number of particles. This additional term preserves the QMBS subspace, yet if $[\hat{Q}^+\hat{Q}^-, \hat{Q}^+] \propto c_+\hat{Q}^+ + c_-\hat{Q}^-$ (for complex coefficients c_\pm), then it also generates nonlinear evolution. In the Appendix, we show that a Hamiltonian term of the form \hat{H}_{nl} can emerge naturally in the scar subspace through a linear coupling of the system to a highly detuned ancillary system. However, there are many other schemes for the dynamical generation of multipartite entanglement [33,48–53].

To illustrate these ideas, we now provide a concrete example of a Hamiltonian with QMBS within the SGA framework.

III. MODEL

Consider a system of spin-1 particles on a d -dimensional cubic lattice with the Hamiltonian $\hat{H}(\eta) = \hat{H}_0 + \hat{H}_{\text{int}}(\eta)$, where

$$\hat{H}_0 = \frac{\omega}{2} \sum_{\vec{n}} \hat{S}_{\vec{n}}^z, \quad (6)$$

$$\hat{H}_{\text{int}}(\eta) = \sum_{\vec{n} > \vec{n}'} \lambda_{\vec{n}, \vec{n}'} (e^{i\eta} \hat{S}_{\vec{n}}^+ \hat{S}_{\vec{n}'}^- + e^{-i\eta} \hat{S}_{\vec{n}}^- \hat{S}_{\vec{n}'}^+). \quad (7)$$

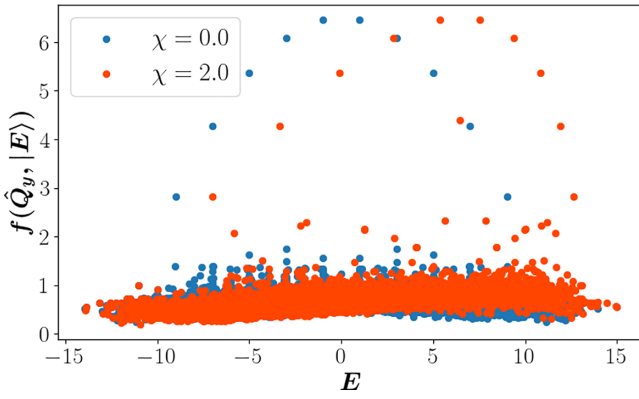


FIG. 1. The QFI density for the eigenstates $|E\rangle$ of the Hamiltonian \hat{H} in Eqs. (6) and (7) (in its zero-momentum symmetry sector) and for the local observable $\hat{Q}^y = \frac{i}{2}(\hat{Q}^- - \hat{Q}^+)$. The QMBS have much larger QFI density than the thermal eigenstates. For $\chi = 0$ (blue), the QMBS are equally spaced in energy, but $\chi \neq 0$ (red) breaks the harmonic energy spacing. Parameters: $N = 11$, $\omega = 2$, $\lambda = 1$, $\gamma = 2$, $\eta = \pi/2$, $L = 10$, $d = 1$. For clarity in the plotted data, a small Hamiltonian perturbation $\hat{H}_{\text{pert}} = 10^{-5}\hat{Q}^x$ is also included here to break some degeneracies due to magnetization symmetry of \hat{H} .

Here, $\hat{S}_{\vec{n}}^{\pm}$ are the spin-1 raising and lowering operators for the particle at the lattice site labeled $\vec{n} \in \mathbb{Z}^d$, and $[\hat{S}_{\vec{n}}^+, \hat{S}_{\vec{n}'}^-] = \delta_{\vec{n}, \vec{n}'} \hat{S}_{\vec{n}}^z$. For convenience, we assume that this interaction term has a power-law decay $\lambda_{\vec{n}, \vec{n}'} = \lambda/(a|\vec{n} - \vec{n}'|)^\gamma$, where $a|\vec{n} - \vec{n}'|$ is the distance between the particles at sites \vec{n} and \vec{n}' on the lattice, a is the lattice spacing, and γ is the range of the power-law decay [54]. If we assume that the lattice is contained in a fixed volume $V = L^d$, then the total number of particles, $N = (L/a + 1)^d \stackrel{L \gg a}{\approx} V/a^d$, can only be increased by decreasing the lattice spacing a which, however, also results in an increased interaction strength $\lambda_{\vec{n}, \vec{n}'}$. An analysis of the energy level spacing statistics in a symmetry-resolved subspace of $\hat{H}(\eta)$ shows that the Hamiltonian is quantum chaotic for all values of the phase η [31]. However, for $\eta = \pm\pi/2$, the term \hat{H}_{int} is a Dzyaloshinskii-Moriya interaction (DMI) and the total Hamiltonian has a set of $N + 1$ quantum many-body scars $|\mathcal{S}_j\rangle = \mathcal{N}_j(\hat{Q}^+)^j |S_0\rangle$, with

$$\hat{Q}^+ = \sum_{\vec{n}} (\hat{S}_{\vec{n}}^+)^2, \quad |S_0\rangle = \bigotimes_{\vec{n}} |S_{\vec{n}}^z = -1\rangle. \quad (8)$$

In this case, $\hat{H}(\eta = \pm\pi/2)$ fits within the SGA framework described above [cf. Eq. (1)] and the QMBS at nonzero energy density have an extensive multipartite entanglement (see blue markers in Fig. 1). We note that the scarred Hamiltonian $\hat{H}(\eta = \pm\pi/2)$ is closely related to another spin-1 model that is known to host QMBS: The spin-1 XY magnet [55,56].

It is straightforward to show that the operator \hat{Q}^+ given in Eq. (8), along with \hat{Q}^- and $\hat{Q}^z = \frac{1}{2}[\hat{Q}^+, \hat{Q}^-] = \frac{1}{2} \sum_{\vec{n}} \hat{S}_{\vec{n}}^z$, form an SU(2) algebra. The corresponding SU(2) spin-coherent states $|\theta, \phi\rangle = \bigotimes_{\vec{n}} [\cos \frac{\theta}{2} |-1_{\vec{n}}\rangle + e^{-i\phi} \sin \frac{\theta}{2} |1_{\vec{n}}\rangle]$ are separable product states of the spins. Preparing such a state initially and allowing it to evolve by $\hat{H}(\eta = \pm\pi/2)$ leads to periodic revivals and the system remains in a product state

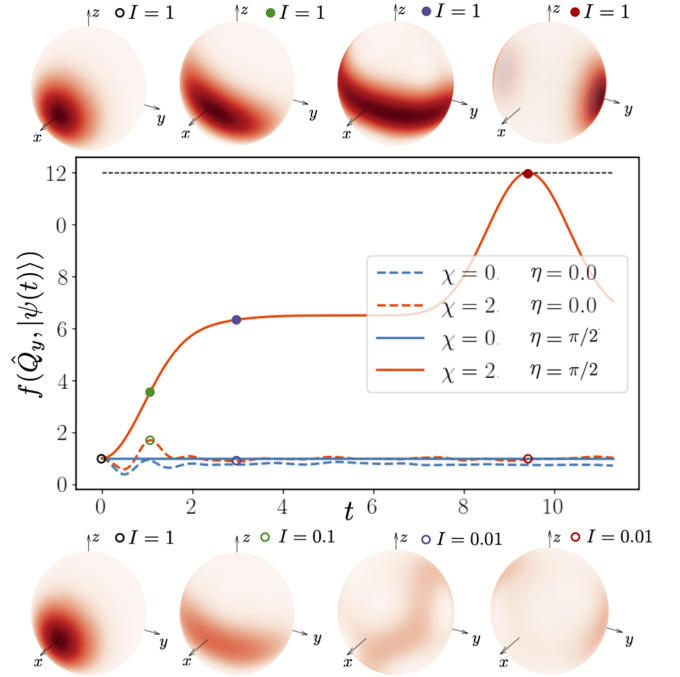


FIG. 2. The evolution of the QFI density by the Hamiltonian \hat{H} , with the initial product state $|\psi(0)\rangle = |\theta = \frac{\pi}{2}, \phi = 0\rangle = \bigotimes_{\vec{n}} [(|+1_{\vec{n}}\rangle + |-1_{\vec{n}}\rangle)/\sqrt{2}]$. Without QMBS ($\eta = 0$), the dynamics never generates states with large f . For the Hamiltonian with QMBS ($\eta = \pi/2$), the QFI density remains small for $\chi = 0$, but $\chi \neq 0$ generates a variety of highly multipartite entangled states. The dashed black line indicates the Heisenberg limit, $f = N$. Above and below the plot are Husimi distributions (in the Dicke subspace) for states at various times in the dynamics (above for $\eta = \pi/2$, below for $\eta = 0$). Parameters: $N = 12$, $\omega = 0$, $\lambda = 1$, $\gamma = 2$, $L = 10$, $d = 1$.

throughout the dynamics. This is reflected by the small, constant value of the QFI density as a function of time (see Fig. 2, solid blue line). So, despite the extensive multipartite entanglement of the QMBS, the dynamics involves only product states. For comparison, we also show the dynamics of the QFI density for evolution by the Hamiltonian $\hat{H}(\eta = 0)$, i.e., for a similar model without QMBS. In that case, the system approaches a thermalized state with $f \sim 1$ (Fig. 2, dashed blue line).

IV. DYNAMICAL GENERATION OF ENTANGLEMENT

We now consider the addition of the nonlinear term given by Eq. (5) to our model $H(\eta)$. The total Hamiltonian thus reads

$$\hat{H}_{\text{tot}}(\eta) = \hat{H}(\eta) + \hat{H}_{\text{nl}} = \hat{H}(\eta) + \frac{\chi}{N} \hat{Q}^+ \hat{Q}^-, \quad (9)$$

where \hat{Q}^+ is the raising operator in the QMBS subspace defined in Eq. (8). Figure 1 (red markers) shows the QFI density of the eigenstates of the scarred Hamiltonian $\hat{H}_{\text{tot}}(\eta = \pm\pi/2)$. We see that the addition of the nonlinear term preserves the existence of the QMBS, and their high QFI density, but destroys the harmonic spacing between them. Thus, upon dynamics from a spin-coherent state, it will generate a variety

of multipartite entangled states. Using the $SU(2)$ commutation relations, \hat{H}_{nl} can be rewritten as $\hat{H}_{\text{nl}} = \frac{\chi}{N}[\hat{Q}^2 - (\hat{Q}^z)^2 + \hat{Q}^z]$, where $\hat{Q}^2 = \frac{1}{2}\{\hat{Q}^+, \hat{Q}^-\} + (\hat{Q}^z)^2$. The one-axis twisting term $\sim(\hat{Q}^z)^2$ is well known to dynamically generate multipartite entanglement in collective spin systems [57–61]. Here, we show how this also holds in a many-body system with local interactions, provided that its Hamiltonian has QMBS. We initialize in a coherent state

$$|\psi_0\rangle = \left| \theta = \frac{\pi}{2}, \phi = 0 \right\rangle = \bigotimes_{\bar{n}} \frac{|+1_{\bar{n}}\rangle + |-1_{\bar{n}}\rangle}{\sqrt{2}} \quad (10)$$

and consider its evolution with the total Hamiltonian $\hat{H}_{\text{tot}}(\eta)$. Figure 2 (red line) shows that the addition of the new term $\hat{H}_{\text{nl}} = \frac{\chi}{N}\hat{Q}^+\hat{Q}^-$ dynamically generates highly multipartite entangled states. After an initial transient, the QFI of $|\psi(t)\rangle$ becomes compatible with that of a Dicke state whose QFI is superextensive with N , in particular, $f = N/2$. We also notice that at large times $t^* \sim N/\chi$, quantum interference effects lead to the generation of macroscopic cat states, also known as the Greenberger-Horne-Zeilinger (GHZ) state, for which the Heisenberg limit $f(t^*) = N$ is reached [15,58,60,61]. For comparison, we also show the dynamics of the QFI density for the corresponding model without QMBS at $\eta = 0$ (dashed red line). In this case, the QFI density is $f \sim 1$, indicating that the QMBS are crucial for generating multipartite entanglement in this model, starting from the same spin-coherent state.

This dynamical protocol is the key insight of the paper and it can be visualized on the generalized Bloch sphere identified by the $SU(2)$ algebra. States that overlap with the scars can be represented by the Husimi distribution $Q(\theta, \phi) = |\langle \psi | \theta, \phi \rangle|^2$, where $|\theta, \phi\rangle$ is a coherent state on the sphere. The Q is characterized by the property that its integral,

$$I = \frac{N}{4\pi} \int d\theta d\phi \sin\theta Q(\theta, \phi), \quad (11)$$

is normalized ($I = 1$) for states that live only on the Bloch sphere, while, in general, $0 \leq I \leq 1$. Hence, I quantifies the localization of the state on the scarred subspace. In the absence of QMBS (bottom panel of Fig. 2), the initial coherent state spreads over all the Hilbert space and leaves the Bloch sphere, as shown by $I(t) < 1$. On the other hand, when the state is evolved with $\hat{H}_{\text{tot}}(\eta = \pi/2)$ (upper panel of Fig. 2), the Q displays evolution with $I(t) = 1$: It initially undergoes squeezing (green marker), then spreads on the equator (purple marker), and eventually exhibits a GHZ state at t^* (red marker).

Another advantage of the generation of highly multipartite states using QMBS is shown by considering finite volume effects in realistic protocols. In our model Hamiltonian, we have assumed that the spins are on a square lattice with a fixed volume V . To increase the number of particles in the fixed volume therefore means increasing their density, which results in stronger interactions. Typically, this limits the size of the multipartite entangled state that can be generated in the dynamics. This is shown in Fig. 3. We see that for small N (corresponding to a low density of particles), the QFI density that can be achieved actually approaches the Heisenberg limit $f = N$ for any value of η . However, in the absence of QMBS, larger values of N (corresponding to an increased particle

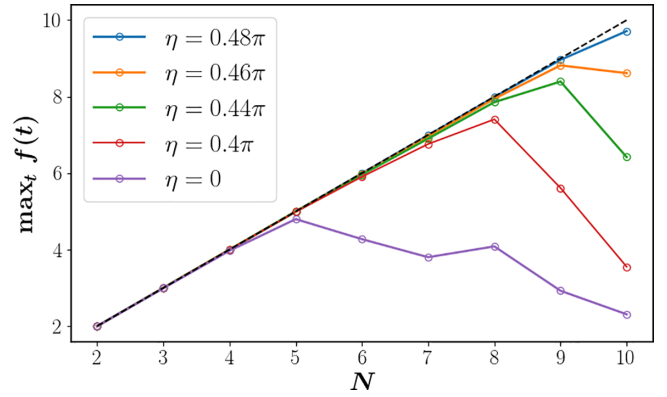


FIG. 3. The largest QFI density $\max_t f(t) = \max_t f(\hat{Q}_y, |\psi(t)\rangle)$ that can be generated dynamically in a system of N spins constrained to a fixed volume $V = L^d$. Since the volume is fixed, increasing the system size N leads to higher density and stronger interactions, and inhibits the growth of the QFI density in the absence of QMBS. The dashed black line shows the Heisenberg limit $f = N$. Parameters: $\omega = 1$, $\chi = 2$, $\lambda = 1$, $\gamma = 2$, $d = 1$, $\theta = \pi/2$, $\phi = 0$.

density) result in stronger interactions between the particles that inhibit the size of the multipartite entangled state. On the contrary, for a Hamiltonian with perfect QMBS ($\phi = \pm\eta/2$), the size of the multipartite entangled state can grow with the Heisenberg scaling $f \sim N$ despite the stronger interactions.

V. ENTANGLEMENT-ENHANCED QUANTUM METROLOGY

The quantum Fisher information gives a bound to the estimation error that is only achievable for an optimal measurement. However, such optimal measurements are often impractical, particularly for large multipartite entangled states. Following Ref. [62], we propose that the multipartite entanglement generated in our model can be exploited for quantum metrology by a feasible “echo” measurement [63–67]. We focus on our spin-1 model and—to slightly simplify our scheme—we choose $\omega = -\chi/N$ (since this gives cancellation between the terms proportional to $\hat{Q}^z = \frac{1}{2}\sum_{\bar{n}} \hat{S}_{\bar{n}}^z$ that appear in \hat{H}_0 and $\hat{H}_{\text{nl}} = \frac{\chi}{N}\hat{Q}^+\hat{Q}^- = \frac{\chi}{N}[\hat{Q}^2 - (\hat{Q}^z)^2 + \hat{Q}^z]$). The scheme is as follows. (i) State preparation: Starting from the spin-coherent state $|\theta = \frac{\pi}{2}, \phi = 0\rangle$, evolve for a time t by the total Hamiltonian, corresponding to the unitary $\hat{U}(\omega, \chi) = e^{-it[\hat{H}_0(\omega) + \hat{H}_{\text{int}} + \hat{H}_{\text{nl}}(\chi)]}$. Note that this is a quantum chaotic Hamiltonian whose dynamics, in the absence of QMBS, is expected to lead to thermalization. (ii) Parameter encoding: Implement a unitary rotation via $\hat{U}_\varepsilon = e^{i\varepsilon\hat{Q}_y}$, where $\varepsilon \approx 0$ is the small parameter to be estimated. (iii) Echo measurement step: Evolve for another time period t by the total Hamiltonian, but with the signs of ω and χ reversed, i.e., by the unitary $\hat{U}(-\omega, -\chi)$. Note that the interaction term \hat{H}_{int} , which is responsible for potentially damaging interactions between the spins, is not reversed. (iv) Readout: Finally, measure the observable \hat{Q}_y .

The final state after the evolution in steps (i)–(iii) is $|\psi(2t)\rangle = \hat{U}(-\omega, -\chi)e^{i\varepsilon\hat{Q}_y}\hat{U}(\omega, \chi)|\xi\rangle$. For the observable measured in step (iv), the mean-squared error in the estimate

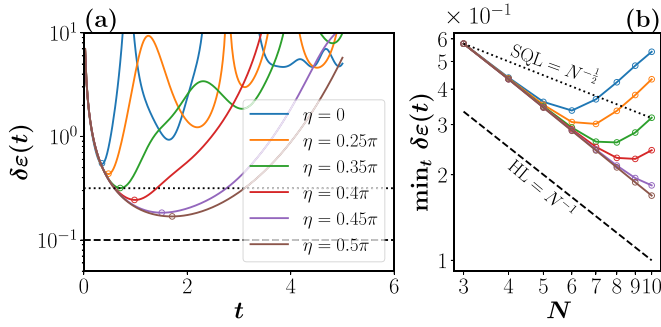


FIG. 4. The estimation error $\delta\epsilon$ using a state prepared in our system of spin-1 particles constrained to a fixed volume $V = L^d$. Left: The error fails to reach even the the standard quantum limit (dotted black line, $\text{SQL} = N^{-1/2}$) when $\eta \approx 0$, due to thermalization of the spin-1 system. However, entanglement-enhanced estimation is possible when the model has QMBS ($\eta \approx \pi/2$) (plotted for $N = 10$ spins). Right: Due to the volume constraint, strong interactions between the spins typically inhibit the achievable error as the system size increases. However, for perfect QMBS, the error decreases uninhibited with the Heisenberg scaling $\sim N^{-1}$ (dashed black line). Parameters: $L = 10$, $\omega = -\chi/N$, $\chi = 2$, $\lambda = 1$, $\gamma = 2$, $d = 1$.

of the parameter is

$$\delta\epsilon = \left| \frac{\sqrt{\text{Var}_{|\psi(2t)\rangle} \hat{Q}_y}}{\partial_\epsilon \langle \hat{Q}_y \rangle} \right|_{\epsilon=0}. \quad (12)$$

Figure 4(a) shows this error as a function of the state preparation time t for different values of the phase η appearing in \hat{H}_{int} . When $\eta \approx 0$, the precision fails to reach even the standard quantum limit (dotted black line) due to thermalization of the system during the state preparation and echo stages. However, we see significantly entanglement-enhanced estimation (i.e., beating the standard quantum limit) when the model has perfect QMBS at $\eta \approx \pm\pi/2$. Similarly, Fig. 4(b) shows that due to the constraint that the spin system is confined to a fixed volume V , the precision is inhibited by interactions between the particles as the particle number N (and hence the density N/V) is increased. On the other hand, the precision is enhanced with the Heisenberg scaling $\delta\epsilon \sim 1/N$ when the model has perfect QMBS.

VI. ROBUSTNESS

Although our metrological scheme is robust to interactions of the form given in Eq. (7) with $\eta = \pi/2$, it is important to examine the robustness of our scheme to deviations from this perfect scar point. For example, Fig. 4(b) shows that to obtain a given level of estimation error, the fine tuning of η needs to be more and more precise as the system size N increases. To quantify this, we numerically calculate the detuning $\delta\eta_{\text{SQL}} = \frac{\pi}{2} - \eta_{\text{SQL}}$ that is needed to give sensing at the standard quantum limit, where η_{SQL} is defined by $\min_t \delta\epsilon(t, \eta_{\text{SQL}}) = N^{-1/2} = \text{SQL}$. In other words, η should be fine tuned within $\delta\eta_{\text{SQL}}$ of $\eta = \pi/2$ to beat the SQL. The results are plotted in Fig. 5 for a given set of system parameters.

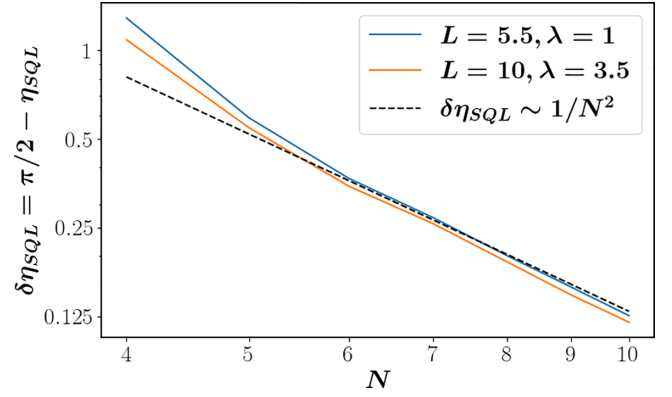


FIG. 5. The deviation from the perfectly fine-tuned scar point $\eta = \pi/2$ that is required to achieve sensing at the standard quantum limit (SQL) in a system of spin-1 particles confined to a volume $V = L^d$. Parameters: $\omega = -\chi/N$, $\chi = 2$, $\gamma = 2$, $d = 1$.

Unfortunately, our exact numerical simulations are restricted to relatively small system sizes (due to the exponentially increasing dimension of the state space). However, Fig. 5, for $N \leq 10$, suggests a scaling $\delta\eta_{\text{SQL}} \sim N^{-2}$, with a fine tuning better than $\delta\eta_{\text{SQL}} \sim 0.1$ needed to beat the SQL for $N \sim 10$ (for our particular choice of system parameters). If this scaling can be extrapolated to larger system sizes, then with $N \sim 30$, a fine tuning better than $\delta\eta_{\text{SQL}} \sim 0.01$ is needed, and with $N \sim 100$, a fine tuning better than $\delta\eta_{\text{SQL}} \sim 0.001$ is required. This shows that the level of fine tuning may be feasible for intermediate size systems, but eventually becomes infeasible for large systems. However, we note that large- N entanglement-enhanced metrology in the presence of generic local interactions is a difficult and longstanding problem and, to the best of our knowledge, there are no existing alternative protocols that can solve this problem without fine tuning or some similarly demanding engineering requirement. Our scheme is a different approach to the problem that we believe can complement existing methods, such as dynamical decoupling [31,68].

VII. DISCUSSION

In this work, we have presented a scheme to generate highly multipartite entangled states, even in the presence of strong local interactions, by exploiting quantum many-body scars. Scars are currently the focus of great attention; however, apart from examples that do not exploit entanglement [31], potential applications are still mostly lacking. Here, we have proposed a metrological scheme which relies on the existence of the scars for entanglement-enhanced phase estimation.

Our scheme is applicable to any model with QMBS in the SGA framework, provided that a multipartite entanglement generating term can be implemented (e.g., as outlined in the Appendix). In terms of practical implementation, most experiments showing evidence of QMBS so far have emulated the PXP model [17,19], which does not straightforwardly fit into the SGA framework discussed here. However, the QMBS subspace in the PXP model has an approximate $\text{SU}(2)$ structure [69] and our scheme should also be applicable there, given an appropriate term to generate multipartite entanglement in the QMBS subspace. Alternatively, evolution with the bare

XP Hamiltonian can generate multipartite entangled states at intermediate times [30] and, using the prescription outlined in this work, it can be stabilized and used for quantum-enhanced metrology.

Finally, we note that several recent works have shown that some types of local interactions can actually generate multipartite entanglement [33,51–53]. In our work, we take a different perspective: We consider local interactions that tend to destroy multipartite entanglement. The main role of QMBS is then to provide robustness to these local interactions that, on first glance, might be expected to rapidly thermalize the system. We believe that the framework outlined in our work will inspire future works in quantum engineering of nonergodic subspaces for applications in quantum technologies.

ACKNOWLEDGMENTS

J.G. is supported by a SFI-Royal Society University Research Fellowship and acknowledges funding from European Research Council Starting Grant ODYSSEY (Grant Agreement No. 758403). S.P. is supported by the Simons Foundation Grant No. 454943. S.D. acknowledges financial support from the SFI-EPSC joint project QuamNESS. S.P. has received funding from the European Union's Horizon Europe program under the Marie Skłodowska Curie Action VERMOUTH (Grant No. 101059865).

APPENDIX: DERIVATION OF THE NONLINEAR HAMILTONIAN TERM

As discussed in the main text, the SGA framework of QMBS consists of a subspace $\mathcal{S} \subset \mathcal{H}$ of the Hilbert space, and an operator \hat{Q}^+ that preserves the subspace and obeys the quasiparticle creation property

$$\hat{\mathcal{P}}_{\mathcal{S}}([\hat{H}, \hat{Q}^+] - \omega\hat{Q}^+)\hat{\mathcal{P}}_{\mathcal{S}} = 0. \quad (\text{A1})$$

Here we show that within the general SGA framework, the nonlinear entanglement generation term $\hat{H}_{\text{nl}} = \frac{\chi}{N}\hat{Q}^+\hat{Q}^-$ can emerge naturally in the scar subspace through a linear coupling to a highly detuned ancillary system [71,72].

To see this, consider a linear interaction with a bosonic mode of the form

$$\hat{H}' = \hat{H} + \omega_a \hat{a}^\dagger \hat{a} + J(\hat{Q}^+ \hat{a} + \hat{Q}^- \hat{a}^\dagger), \quad (\text{A2})$$

where \hat{a}^\dagger, \hat{a} are the bosonic creation and annihilation operators and ω_a is the frequency of the mode. Following Ref. [73], we consider the rotated Hamiltonian $e^{\hat{R}}\hat{H}'e^{-\hat{R}}$, where $\hat{R} = \frac{J}{\omega - \omega_a}(\hat{Q}^+ \hat{a} - \hat{Q}^- \hat{a}^\dagger)$. For a small rotation with $J \ll N|\omega - \omega_a|$, we can expand to second order in the small parameter,

$$e^{\hat{R}}\hat{H}'e^{-\hat{R}} \approx \hat{H}' + [\hat{R}, \hat{H}'] + \frac{1}{2}[\hat{R}, [\hat{R}, \hat{H}']] + \dots$$

Restricting to the scar subspace and using Eq. (A1) then allows us to derive an effective Hamiltonian,

$$\begin{aligned} \hat{\mathcal{P}}_{\mathcal{S}}(e^{\hat{R}}\hat{H}'e^{-\hat{R}})\hat{\mathcal{P}}_{\mathcal{S}} \approx & \hat{\mathcal{P}}_{\mathcal{S}} \left[\hat{H} + \omega_a \hat{a}^\dagger \hat{a} + \frac{J^2}{\omega_a - \omega} \hat{Q}^+ \hat{Q}^- \right. \\ & \left. + \frac{J^2}{\omega_a - \omega} [\hat{Q}^+, \hat{Q}^-] \hat{a}^\dagger \hat{a} \right] \hat{\mathcal{P}}_{\mathcal{S}}. \end{aligned} \quad (\text{A3})$$

If we also assume that the ancillary mode is in its vacuum state $\hat{a}^\dagger \hat{a} = 0$, then we finally have

$$\hat{H}_{\text{eff}} = \hat{\mathcal{P}}_{\mathcal{S}} \left[\hat{H} + \frac{J^2}{\omega_a - \omega} \hat{Q}^+ \hat{Q}^- \right] \hat{\mathcal{P}}_{\mathcal{S}} \quad (\text{A4})$$

in the scar subspace. Note that the strength of the nonlinear term is $J^2/(\omega_a - \omega) \sim \mathcal{O}(1/N)$ due to the approximation condition $NJ \ll |\omega - \omega_a|$. Defining $\chi = NJ^2/(\omega_a - \omega)$ makes this dependence on N explicit and gives the desired nonlinear term $\hat{H}_{\text{nl}} = \frac{\chi}{N}\hat{Q}^+\hat{Q}^-$.

There are various imperfections that can arise in a realistic system that cause deviations from the effective Hamiltonian given by (A4), for example, higher-order terms in the expansion given by Eq. (A3), spatial inhomogeneity in the spin frequencies ω , or spatial inhomogeneity in the couplings J . Several of these imperfections are discussed in detail in Ref. [72] where, for instance, it is shown that the effect of higher-order terms can be suppressed by dissipation in the ancillary system.

-
- [1] L. D'Alessio, Y. Kafri, A. Polkovnikov, and M. Rigol, *Adv. Phys.* **65**, 239 (2016).
- [2] T. Mori, T. N. Ikeda, E. Kaminishi, and M. Ueda, *J. Phys. B: At., Mol. Opt. Phys.* **51**, 112001 (2018).
- [3] P. Calabrese and J. Cardy, *J. Stat. Mech.: Theory Expt.* (2005) P04010.
- [4] G. D. Chiara, S. Montangero, P. Calabrese, and R. Fazio, *J. Stat. Mech.: Theory Expt.* (2006) P03001.
- [5] H. Kim and D. A. Huse, *Phys. Rev. Lett.* **111**, 127205 (2013).
- [6] D. N. Page, *Phys. Rev. Lett.* **71**, 1291 (1993).
- [7] D. Gross, S. T. Flammia, and J. Eisert, *Phys. Rev. Lett.* **102**, 190501 (2009).
- [8] G. Tóth, *Phys. Rev. A* **85**, 022322 (2012).
- [9] P. Hyllus, W. Laskowski, R. Kriscsek, C. Schwemmer, W. Wiczołek, H. Weinfurter, L. Pezzè, and A. Smerzi, *Phys. Rev. A* **85**, 022321 (2012).
- [10] L. Pezzè and A. Smerzi, *Phys. Rev. Lett.* **102**, 100401 (2009).
- [11] S. L. Braunstein and C. M. Caves, *Phys. Rev. Lett.* **72**, 3439 (1994).
- [12] V. Giovannetti, S. Lloyd, and L. Maccone, *Nat. Photon.* **5**, 222 (2011).
- [13] M. G. Paris, *Intl. J. Quantum Inf.* **07**, 125 (2009).
- [14] D. Petz and C. Ghinea, in *Quantum Probability and Related Topics*, edited by R. Robolledo and M. Orszag (World Scientific, 2011), Vol. 27, pp. 261–281.
- [15] L. Pezzè, A. Smerzi, M. K. Oberthaler, R. Schmied, and P. Treutlein, *Rev. Mod. Phys.* **90**, 035005 (2018).
- [16] M. J. Holland and K. Burnett, *Phys. Rev. Lett.* **71**, 1355 (1993).
- [17] H. Bernien, S. Schwartz, A. Keesling, H. Levine, A. Omran, H. Pichler, S. Choi, A. S. Zibrov, M. Endres, M. Greiner *et al.*, *Nature (London)* **551**, 579 (2017).
- [18] D. Bluvstein, A. Omran, H. Levine, A. Keesling, G. Semeghini, S. Ebadi, T. T. Wang, A. A. Michailidis, N. Maskara, W. W. Ho, S. Choi, M. Serbyn, M. Greiner, V. Vuletić, and M. D. Lukin, *Science* **371**, 1355 (2021).

- [19] G.-X. Su, H. Sun, A. Hudomal, J.-Y. Desaulles, Z.-Y. Zhou, B. Yang, J. C. Halimeh, Z.-S. Yuan, Z. Papić, and J.-W. Pan, Observation of unconventional many-body scarring in a quantum simulator (unpublished).
- [20] P. Zhang, H. Dong, Y. Gao, L. Zhao, J. Hao, Q. Guo, J. Chen, J. Deng, B. Liu, W. Ren, Y. Yao, X. Zhang, S. Xu, K. Wang, F. Jin, X. Zhu, H. Li, C. Song, Z. Wang, F. Liu, Z. Papić, L. Ying, H. Wang, and Y.-C. Lai, Many-body Hilbert space scarring on a superconducting processor (unpublished).
- [21] C. J. Turner, A. A. Michailidis, D. A. Abanin, M. Serbyn, and Z. Papić, *Nat. Phys.* **14**, 745 (2018).
- [22] M. Serbyn, D. A. Abanin, and Z. Papić, *Nat. Phys.* **17**, 675 (2021).
- [23] S. Moudgalya, B. A. Bernevig, and N. Regnault, *Rep. Prog. Phys.* **85**, 086501 (2022).
- [24] N. Shiraishi and T. Mori, *Phys. Rev. Lett.* **119**, 030601 (2017).
- [25] S. Dooley and G. Kells, *Phys. Rev. B* **102**, 195114 (2020).
- [26] Z. Papić, *Entanglement in Spin Chains: From Theory to Quantum Technology Applications*, edited by A. Bayat, S. Bose, and H. Johannesson (Springer International Publishing, 2022), pp. 341–395.
- [27] S. Dooley and G. Kells, *Phys. Rev. B* **105**, 155127 (2022).
- [28] F. Schindler, N. Regnault, and B. A. Bernevig, *Phys. Rev. B* **105**, 035146 (2022).
- [29] A. Chandran, T. Iadecola, V. Khemani, and R. Moessner, *arXiv:2206.11528*.
- [30] J.-Y. Desaulles, F. Pietracaprina, Z. Papić, J. Goold, and S. Pappalardi, *Phys. Rev. Lett.* **129**, 020601 (2022).
- [31] S. Dooley, *PRX Quantum* **2**, 020330 (2021).
- [32] B. Windt and H. Pichler, *Phys. Rev. Lett.* **128**, 090606 (2022).
- [33] T. Comparin, F. Mezzacapo, and T. Roscilde, *Phys. Rev. A* **105**, 022625 (2022).
- [34] D. K. Mark, C.-J. Lin, and O. I. Motrunich, *Phys. Rev. B* **101**, 195131 (2020).
- [35] S. Moudgalya, N. Regnault, and B. A. Bernevig, *Phys. Rev. B* **102**, 085140 (2020).
- [36] N. O’Dea, F. Burnell, A. Chandran, and V. Khemani, *Phys. Rev. Res.* **2**, 043305 (2020).
- [37] B. Buča, J. Tindall, and D. Jaksch, *Nat. Commun.* **10**, 1730 (2019).
- [38] M. Medenjak, B. Buča, and D. Jaksch, *Phys. Rev. B* **102**, 041117(R) (2020).
- [39] C. W. Helstrom, *J. Stat. Phys.* **1**, 231 (1969).
- [40] G. Tóth and I. Apellaniz, *J. Phys. A: Math. Theor.* **47**, 424006 (2014).
- [41] L. Pezzè and A. Smerzi, *arXiv:1411.5164*.
- [42] P. Hauke, M. Heyl, L. Tagliacozzo, and P. Zoller, *Nat. Phys.* **12**, 778 (2016).
- [43] S. Pappalardi, A. Russomanno, A. Silva, and R. Fazio, *J. Stat. Mech.: Theory Expt.* (2017) 053104.
- [44] M. Brenes, S. Pappalardi, J. Goold, and A. Silva, *Phys. Rev. Lett.* **124**, 040605 (2020).
- [45] P. Laurell, A. Scheie, C. J. Mukherjee, M. M. Koza, M. Enderle, Z. Tylczynski, S. Okamoto, R. Coldea, D. A. Tennant, and G. Alvarez, *Phys. Rev. Lett.* **127**, 037201 (2021).
- [46] A. Scheie, P. Laurell, A. M. Samarakoon, B. Lake, S. E. Nagler, G. E. Granroth, S. Okamoto, G. Alvarez, and D. A. Tennant, *Phys. Rev. B* **103**, 224434 (2021).
- [47] R. Costa de Almeida and P. Hauke, *Phys. Rev. Res.* **3**, L032051 (2021).
- [48] M. Mamaev, I. Kimchi, R. M. Nandkishore, and A. M. Rey, *Phys. Rev. Res.* **3**, 013178 (2021).
- [49] M. Płodzień, M. Kościelski, E. Witkowska, and A. Sinatra, *Phys. Rev. A* **102**, 013328 (2020).
- [50] T. Hernández Yanes, M. Płodzień, M. Mackoīt Sinkevičienė, G. Žlabys, G. Juzeliūnas, and E. Witkowska, *Phys. Rev. Lett.* **129**, 090403 (2022).
- [51] M. A. Perlin, C. Qu, and A. M. Rey, *Phys. Rev. Lett.* **125**, 223401 (2020).
- [52] T. Comparin, F. Mezzacapo, M. Robert-de-Saint-Vincent, and T. Roscilde, *Phys. Rev. Lett.* **129**, 113201 (2022).
- [53] J. T. Young, S. R. Muleady, M. A. Perlin, A. M. Kaufman, and A. M. Rey, Enhancing spin squeezing using soft-core interactions (unpublished).
- [54] The double sum in Eq. (7) is over a restricted set of lattice sites, denoted $\bar{n} > \bar{n}'$, to avoid a redundant repetition of terms in the sum.
- [55] M. Schecter and T. Iadecola, *Phys. Rev. Lett.* **123**, 147201 (2019).
- [56] The two models are related by a unitary transformation if the graph with edges given by nonzero interactions $\lambda_{\bar{n},\bar{n}'}$ is bipartite [70].
- [57] M. Kitagawa and M. Ueda, *Phys. Rev. A* **47**, 5138 (1993).
- [58] G. S. Agarwal, R. R. Puri, and R. P. Singh, *Phys. Rev. A* **56**, 2249 (1997).
- [59] K. Mølmer and A. Sørensen, *Phys. Rev. Lett.* **82**, 1835 (1999).
- [60] S. M. Chumakov, A. Frank, and K. B. Wolf, *Phys. Rev. A* **60**, 1817 (1999).
- [61] S. Dooley and T. P. Spiller, *Phys. Rev. A* **90**, 012320 (2014).
- [62] E. Davis, G. Bentsen, and M. Schleier-Smith, *Phys. Rev. Lett.* **116**, 053601 (2016).
- [63] T. Macrì, A. Smerzi, and L. Pezzè, *Phys. Rev. A* **94**, 010102(R) (2016).
- [64] O. Hosten, R. Krishnakumar, N. J. Engelsen, and M. A. Kasevich, *Science* **352**, 1552 (2016).
- [65] D. Linnemann, H. Strobel, W. Muessel, J. Schulz, R. J. Lewis-Swan, K. V. Kheruntsyan, and M. K. Oberthaler, *Phys. Rev. Lett.* **117**, 013001 (2016).
- [66] S. P. Nolan, S. S. Szigeti, and S. A. Haine, *Phys. Rev. Lett.* **119**, 193601 (2017).
- [67] A. J. Hayes, S. Dooley, W. J. Munro, K. Nemoto, and J. Dunningham, *Quantum Sci. Technol.* **3**, 035007 (2018).
- [68] L. Viola, E. Knill, and S. Lloyd, *Phys. Rev. Lett.* **82**, 2417 (1999).
- [69] S. Choi, C. J. Turner, H. Pichler, W. W. Ho, A. A. Michailidis, Z. Papić, M. Serbyn, M. D. Lukin, and D. A. Abanin, *Phys. Rev. Lett.* **122**, 220603 (2019).
- [70] D. K. Mark and O. I. Motrunich, *Phys. Rev. B* **102**, 075132 (2020).
- [71] S. D. Bennett, N. Y. Yao, J. Otterbach, P. Zoller, P. Rabl, and M. D. Lukin, *Phys. Rev. Lett.* **110**, 156402 (2013).
- [72] S. Dooley, E. Yukawa, Y. Matsuzaki, G. C. Knee, W. J. Munro, and K. Nemoto, *New J. Phys.* **18**, 053011 (2016).
- [73] A. B. Klimov and L. L. Sanchez-Soto, *Phys. Rev. A* **61**, 063802 (2000).